Mw 7.8 Tarapaca intermediate depth earthquake of 13 June 2005 (northern Chile); fault plane identification and slip distribution by waveform inversion

B. Delouis, Denis Legrand

Mw 7.8 Tarapaca intermediate depth earthquake of 13 June 2005 (northern Chile): Fault plane identification and slip distribution by waveform inversion

Bertrand Delouis[1] and Denis Legrand[2]

Received 20 September 2006; revised 20 November 2006; accepted 30 November 2006; published 5 January 2007.

[1] The Mw 7.8 Tarapaca earthquake of 13 June 2005 occurred between 90 and 115 km depth within the subducting slab of northern Chile. The fault plane could be identified using two independent approaches: by locating accurately one week of aftershocks and by modeling the strong-motion waveforms. The rupture occurred on a low-angle (15°) west-dipping plane in pure normal faulting. The slip distribution obtained by the joint inversion of strong-motion and teleseismic data indicates a compact slip zone of dimension 50 × 40 km^2 with a maximum slip of 13 m. The aftershock distribution slightly extends beyond the slip zone dimension in the NS direction but slip extends slightly more towards the west than do the aftershocks. The Tarapaca earthquake can be classified as an intraslab down-dip tensional event, in the context of a mature seismic gap.
Citation: Delouis, B., and D. Legrand (2007), Mw 7.8 Tarapaca intermediate depth earthquake of 13 June 2005 (northern Chile): Fault plane identification and slip distribution by waveform inversion, *Geophys. Res. Lett.*, *34*, L01304, doi:10.1029/2006GL028193.

1. Introduction

[2] On June 13, 2005 (22h44 GMT), the Tarapaca region of northern Chile was struck by a large earthquake of Mw 7.8 with an epicenter located 100 km east-north-east of the city of Iquique (Figure 1 and Table 1), 4 years after the Mw 8.1 Arequipa, southern Peru earthquake. With a source depth in the range 90 to 115 km (Table 1), this event can be categorized as an intermediate depth earthquake, occurring within the subducting Nazca plate according to the Wadati-Benioff zone imaged by *Comte and Suárez* [1995]. In northern Chile, the shallow part of the subduction interface remains essentially unruptured since 1877 and the region is identified as a major seismic gap [*Comte and Pardo*, 1991]. To date, the gap extends approximately from 23°S (Mejillones/Antofagasta) to 18°S (Ilo, southern part of the 2001 Arequipa earthquake, Figure 1). The Tarapaca earthquake occurred in the central part of the remaining seismic gap.

[3] Intermediate depth subduction earthquakes rarely are characterized by a precise aftershock distribution and few have been analysed in terms of slip distribution. Identification of the rupture plane of large subduction earthquakes is relatively straightforward for thrust faulting events occurring along the shallow part of the plate interface. Conversely, the inherent ambiguity between the two nodal planes of the focal mechanism is more difficult to resolve in the case of intraslab intermediate depth earthquakes. This has been successfully done in Japan for some events using accurate aftershock locations, showing that the activated rupture plane could be either nearly horizontal (e.g. 1993 Kushiro-oki earthquake [*Suzuki and Kasahara*, 1996]) or steeply dipping (e.g. 2003 off-shore Miyagi earthquake [*Okada and Hasegawa*, 2003]). In northern Chile, the only known large event of this type is the December 9, 1950, Ms = 8 earthquake which occurred landward of Antofagasta. *Kausel and Campos* [1992] modeled the long-period body waves of this normal faulting event and inferred a near vertical rupture plane, without clear evidence, however, for fault plane discrimination.

[4] This study is motivated by the availability of a rich and diverse data set that allows to investigate the details of this earthquake beyond standard analysis. The 2005 Tarapaca earthquake was well recorded both at teleseismic and local distances by the global array of broadband seismological stations as well as by six digital accelerometers. A temporary network of 9 seismometers was installed in the source area one week after the mainshock for aftershock monitoring. By combining this great variety of seismological data, we located the mainshock hypocenter, determined its focal mechanism, identified the rupture plane, and characterized the slip distribution.

2. Waveform Data

[5] The Tarapaca earthquake is the first large event (M > 7) in northern Chile recorded by the network of digital accelerometers installed in the region since 2001. This network resulted from a joint effort of Swiss federal institutions (DEZA, SED/ETHZ) together with the University of Chile (http://www.cec.uchile.cl/~ragic/ragic.htm). Strong-motion waveform modeling is performed on the displacement seismograms obtained from the acceleration records (Kinemetics Etna with episensors), after double integration in time and bandpass filtering. The six strong-motion stations incorporated in the analysis are situated at epicentral distances ranging from 55 to 370 km (Figure 1). Absolute time at each station, used in the process of locating the mainshock hypocenter, was provided by a GPS receiver.

[6] Twenty Broadband seismograms from the mainshock recorded at teleseismic distances were obtained from the IRIS data center. To accurately constrain the nodal planes of

[1]Géosciences Azur, CNRS (UMR 6526) and University of Nice, Sophia Antipolis, France.
[2]Departamento de Geofisica, Universidad de Chile, Santiago, Chile.

0094-8276/07/2006GL028193

the mainshock focal mechanism we used the whole set of broadband stations but in the inversion for the slip distribution we used a subset of 10 broadband stations well distributed azimuthally (auxiliary material, Figure S1[1]). Teleseismic data are displacement waveforms windowed around the P (vertical) and SH wave train. Data processing includes deconvolution from the instrument response, integration to obtain displacement, equalization to a common magnification and epicentral distance, and band-pass filtering from 0.01 Hz to 0.8 Hz (P waves) or to 0.4 Hz (SH waves). Teleseismic P waveforms exhibit relatively simple shapes, with direct P and surface reflected pP phases well separated by about 25–30 s, a time separation expected for a depth of about 100 km.

3. Mainshock Location and Focal Mechanism

[7] The latitude, longitude, and depth reported for the mainshock are summarized in Table 1. Best double couple solutions from rapid moment tensor inversions (Table 1) exhibit notable discrepancies but coincide in a predominantly normal faulting focal mechanism with a low-angle and a steep dipping nodal planes. To relocate the mainshock hypocenter and to refine its focal mechanism, we proceeded as following. First, we modeled the P and SH broadband waveforms recorded at teleseismic distances with the *Nabelek* [1984] approach for a double couple point source. The velocity model used throughout this study for the source region was previously elaborated at the Department of Geophysics of the University of Chile for locating the background seismicity of the area (P. Pinares, personal communication, 2006). It consists of 5 layers of thicknesses 5, 5, 10, 20, 30 km overlying a half space. P-wave velocities are 5.8, 6.1, 6.6, 7.1, 7.5 and 8.0 km/s respectively. The crustal Vp/Vs ratio is 1.74. With this velocity model a focal depth of 108 ± 5 km was found. Depth is well constrained by the time separation of the P and pP phases. The focal mechanism is well controlled by the combination of P and SH waves. Best fitting nodal planes are: (strike, dip, rake) = (175, 15, −90) and (355, 75, −90), hereafter called the dip15W and dip75E planes respectively. We located the epicenter using the same velocity model and the three closest strong-motion stations (PICA, IQUI, ARIC) which provided clear arrival times for both P and S waves. With a depth fixed to 108 km, as found from the teleseismic modeling, we obtained an epicenter located very close that of the NEIC and to the HCMT centroid (Table 1). A grid-search on the hypocenter location, using the 3 P and 3 S arrival times at the same three strong-motion stations, confirmed a depth of 108 ± 3 km.

4. Aftershock Distribution

[8] One week after the main shock, a temporary network of nine seismological stations was installed by the Departement of Geophysics of the University of Chile, covering the source region (Figure 2). It comprises one broad-band 3-component station and eight short-period stations (four 3-component and four 1-component). We present here the first week of accurately located aftershocks, spanning the period 2006/06/20 to 2006/06/26. From the total of 473 events recorded during this week, we selected 404 which were recorded by a minimum of 5 stations and provided several S phases in addition to the P readings. Only events with a low rms arrival time residual (<0.1 s) were retained. Aftershocks were located with the HYPOCENTER program (SEISAN package [*Lienert et al.*, 1986]), using the same velocity model as previously mentioned. The mean average horizontal and depth errors are equal to 10 km. Larger absolute errors may have to be considered given that the 1D velocity model used is an approximate representation of the real 3D subduction zone.

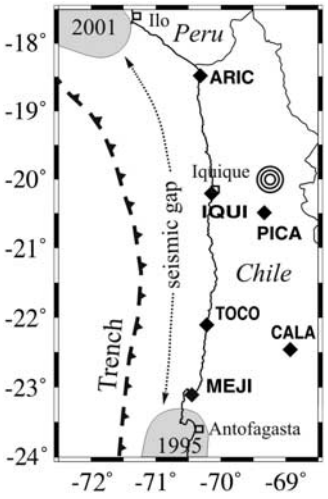

Figure 1. Situation map of northern Chile, southern Peru, with the subduction trench, the terminations of the 2001 Arequipa and 1995 Antofagasta earthquake ruptures (grey surfaces), the remaining seismic gap corresponding to the 1877 rupture, the location of the six strong-motion stations that recorded the mainshock (diamonds ARIC: Arica, IQUI: Iquique, PICA: Pica, TOCO: Tocopilla, CALA: Calama, MEJI: Mejillones), and the 2005 Tarapaca earthquake epicenter (concentric circles).

[9] On the map (Figure 2a), aftershocks define an elongated cluster trending NNW, 60 km long and 30 km wide. In cross-section (Figure 2b), the aftershocks delineate a low angle (10 to 20°) west-dipping plane, with events occurring mainly between 100 and 112 km depth. A similar distribution was obtained by *Peyrat et al.* [2006].

5. Fault Model and Waveform Inversion Procedure

[10] To establish whether the rupture plane can be identified by waveform inversion independently from aftershock data, we initially tested two kinematic source models, one for each nodal plane of the focal mechanism. Kinematic modeling follows the approach of *Delouis et al.* [2002]. The two models initially tested consist of a single fault segment 110 km long and 70 km wide, subdivided into 71 subfaults measuring 10 km along strike and dip. The strike and dip angles of the fault are kept fixed: (strike, dip) = (175°, 15°) for the first model corresponding to nodal plane 1, and (355°, 75°) for nodal plane 2 (Table 1). Seismological data did not show evidence of rake variation and this parameter is fixed to −90° ± 5° (essentially pure normal faulting). In

[1]Auxiliary materials are available in the HTML. doi:10.1029/2006GL028193.

Table 1. Mainshock Location and Focal Mechanism[a]

	Lat., °S	Lon., °W	Prof., km	Strike/Dip/Rake Plane 1	Strike/Dip/Rake Plane 2	Mo, dyne.cm
NEIC/USGS hypocenter	19.99	69.20	115	—–	—–	—–
RESISTE/ARICA hypocenter	19.98	69.42	90	—–	—–	—–
NEIC/USGS centroid	—–	—–	101	231/30/−33	350/75/−116	6.5 E+27
HCMT centroid	20.02	69.23	95	182/23/−81	352/67/−94	5.32 E + 27
This study hypocenter	20.01	69.24	108	175/15/−90	355/75/−90	5.47 E + 27

[a]NEIC/USGS and HCMT centroid planes correspond to best double couple solutions from rapid moment tensor inversion.

all models, rupture initiates at the hypocenter (20.01°S, 69.24°W, 108 km depth). A non linear inversion is performed with a simulated annealing scheme. Subfault source time functions (SSTF) are represented by a single isoscele triangular function of duration 2 s. Details of the SSTF cannot be resolved given the large hypocentral distance (>120 km) and the lowpass filtering of the strong-motion records. Subfault slip onset times are allowed to vary within the interval defined by two bounding rupture velocities, 3.0 and 4.7 km/s.

[11] The cost function to be minimized in the simulated annealing procedure is defined as the weighted sum of the normalized RMS (L2 norm) misfit errors of the two datasets (teleseismic and strong-motion), with an additional function aiming at minimizing the total seismic moment. In the joint inversion, the different datasets were equally weighted. We verified that the main characteristics of the resulting slip model were stable for variable weights. Synthetic seismograms at strong-motion stations are computed using the discrete wavenumber method of *Bouchon* [1981], with the same velocity model as for hypocenter location and teleseismic modeling. Synthetic seismograms at teleseismic stations were generated using ray-theory approximation and the approach by *Nabelek* [1984]. The merit of the joint inversion of strong-motion and teleseismic body waves was well discussed by *Yagi et al.* [2004].

6. Inversion Results

[12] We carried out separate and joint inversions of the teleseismic and strong-motion datasets with both the dip15W and the dip75E fault model. Whatever the fault model, dip15W or dip75E, it resulted difficult to match the teleseismic records at some peculiar stations. A polarity reversal of the synthetic pP phase with respect to the recorded one was observed for stations located to the NNW and to the SSE. The upgoing pP ray path for those stations leave the source in the immediate vicinity of the nodal plane oriented N355 and dipping 75E. Therefore, small heterogeneities in the upper-mantle/crust structure could easily produce a change in the take-off angle of the pP wave implying a change of polarity. This effect cannot be reproduced with a simple 1D-velocity model, and the corresponding stations were discarded from the inversions in order to avoid a possible contamination of the slip models. A different case was that of stations located to the East. At those stations, the initial part of the direct P and pP phases could be easily modeled, but subsequent arrivals in the synthetics had improper amplitude. This could be partially corrected for by increasing the dip of the fault in the lower part of the model.

[13] We found that the low angle west-dipping fault model provided a much better fit of the strong-motion waveforms at PICA and IQUI, the stations closest to the source, than the steep east-dipping fault model (Figures 3a and 3b). This allowed us to identify the low-angle west-dipping plane as the fault plane. Thereafter, the dip 75E fault model is not described.

[14] Our final slip model, producing the best waveform fit in the joint inversion of teleseismic and strong-motion records, comprises two fault segments striking N175 and dipping to the west. The first segment contains the epicenter and dips 15W, while the second, deeper segment is dipping 35W (Figures 2 and 3f).

[15] Modeling of the P and SH waves is shown in Figures 3c and 3d. The improvement of the waveform fit at the eastern stations obtained with the change of dip from 15 to 35° in the deep part of the model (segment 2) is illustrated in Figure 3e. Globally, strong-motion displacement waveforms are correctly modeled (Figure 3a).

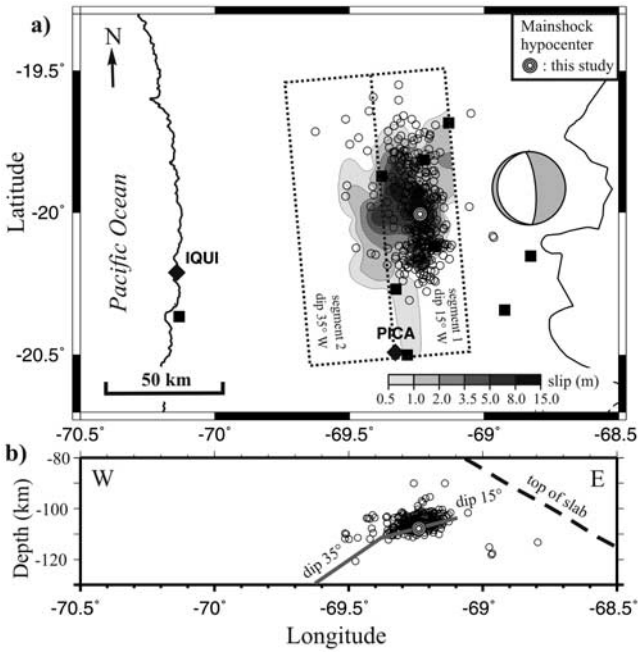

Figure 2. (a) Map and (b) cross-section showing the relationship between the slip model of the mainshock and the aftershocks (open circles). On the map (Figure 2a), the short-dashed lines show the surface projection of the fault model boundaries (maximum authorized area of slip distribution in the model). The focal mechanism is from this study (teleseismic waveform modeling). The position of the two closest strong-motion stations PICA and IQUI is indicated (black diamonds).Temporary stations installed for aftershock monitoring are displayed by black squares. On the cross-section (Figure 2b), the broken grey line represents the 2-segment fault model, and the dashed line indicates the depth of the top of the slab, after *Comte and Suárez* [1995].

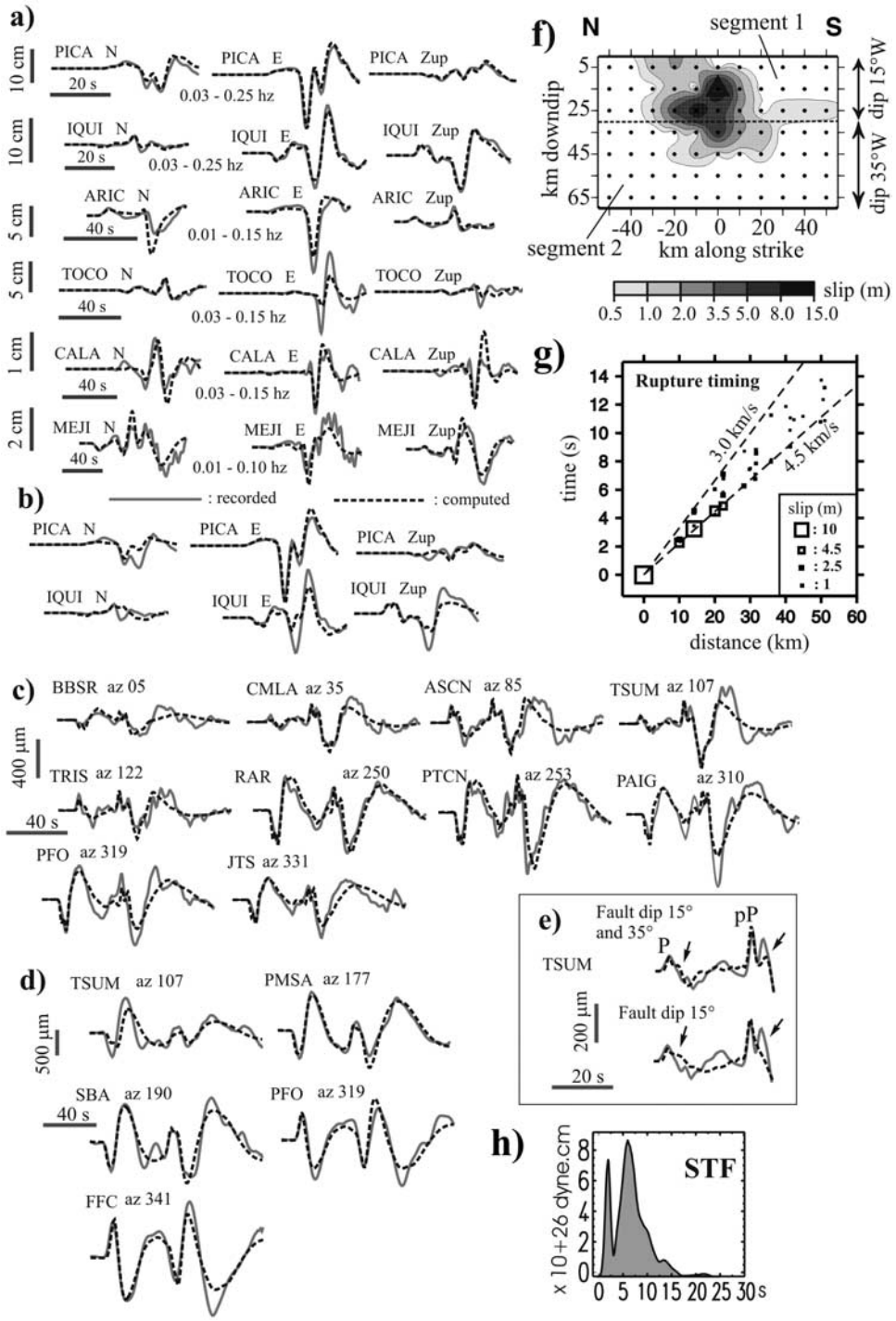

Figure 3. (a) Modeling of the strong-motion displacements for the best slip model with a 2-segment rupture plane dipping 15W and 35W. The range of bandpass filtering is indicated for each station. (b) Modeling with the 75E dipping fault model, shown for stations PICA and IQUI only. (c) Modeling of the P and (d) SH teleseismic waveforms for the same slip model. az: azimuth of the station. (e) Comparison with the modeling obtained using a single fault plane dipping 15W, for the P-wave at station TSUM. Black arrows point to secondary arrivals of P and pP waves whose modeling is improved when dip is increased to 35 degrees in the lowest part of the model (see text for details). (f) Slip map viewed from the direction normal to the fault plane, with hypocenter indicated by the open triangle and subfault centers by black dots. The dashed line is the limit between the two rupture segments of the model. (g) Rupture timing. Each open square represents the slip of an individual subfault, with a size proportional to slip. Dashed lines corresponding to constant rupture velocities 4.5 and 3.0 km/s are drawn for reference. (h) Moment Rate Source Time Function (STF) for the whole rupture. All results from the joint inversion.

[16] The slip distribution is shown in Figure 3f and projected onto the surface in Figure 2a. The main slip area defines a 50×40 km^2 rupture zone, and assuming a mantle rigidity of 7.0×10^{10} Pa, the average slip is 3.9 m. Maximum slip is 13 m, at the hypocenter. Approximating the slip distribution by a circular rupture of radius 25 km, the average static stress drop is 15 MPa (150 bars). The main slip patches are triggered in time according to a rupture velocity close to 4.5 km/s (Figure 3g), corresponding to 97% of the mantle shear-wave velocity. The essential part of the seismic moment is released within 15 s, as shown by the total source time function (STF, Figure 3h). The initial and separated peak in the STF is required by the teleseismic data at stations showing a sharp and narrow initial peak in the P and pP waves (Figure 3c). This feature cannot be reproduced without a high static stress drop at rupture initiation, produced by the 13 m of slip in the hypocentral area.

[17] Slip maps resulting from the separate teleseismic and strong-motion inversions are presented in the auxiliary material (Figure S2). Synthetic resolution tests were carried out in order to assess how the slip distribution was constrained when inverting separately and jointly the teleseismic and strong-motion datasets. Results of those tests (auxiliary material, Figure S3), indicate an improvement of the resolution in the case of the joint inversion, with an acceptable recovering of the main slip characteristics over the entire surface of the fault model. However, the uncertainty on slip values can be estimated to 2–3 m (15–25% of the maximum slip of 13 m, auxiliary material, Figure S4).

7. Discussion and Conclusion

[18] A detailed description of the rupture process of the Mw 7.8 Tarapaca earthquake could be obtained from the combined analysis of the strong-motion and teleseismic records: location of rupture initiation, focal mechanism, identification of the activated fault plane, and slip distribution. Strong-motion data clearly favor the low-angle west dipping fault plane, in agreement with the aftershock data. Teleseismic waveforms point to a moderate increase of the dip of the rupture plane with depth. The essential part of the rupture occurred in a compact slip zone 50×40 km^2, with slip reaching locally 13 m and with a high value of average stress drop (15 MPa). The dominant rupture velocity is 4.5 km/s. Variation of rupture velocity suggested by the timing of low slip subfaults (Figure 3g) is indeed poorly constrained, and we verified that an inversion performed with a rupture velocity fixed to 4.5 km/s provided a comparable waveform fit and slip distribution. Hence, the rupture process was fast, as confirmed by the short duration of the overall source time function (15 s). A steepening of the fault from dip15W to dip35W was found to improve waveform fit at the eastern teleseismic stations. However, a rupture plane having a constant dip of 15W provides an equivalent fit of all other teleseismic and strong-motion stations (auxiliary material, Figure S5). Hence, it could be alternatively proposed that the rupture maintained a constant dip of 15° and that the mismatch at eastern teleseismic stations could be related to a specific effect of the real 3D Earth structure.

[19] The slip distribution and aftershock pattern exhibit a clear degree of coincidence (Figure 2), although there is not a simple and unique spatial correlation between slip magnitude and aftershock density (Figure 2a). A group of aftershocks coincide with large slip at the hypocenter, but north and south of that point the majority of aftershocks are located in areas of low slip, at the margin of the main asperity. The lateral (NS) extension of the main cluster of densely grouped aftershocks slightly surpasses the dimension of the slip area. Remarkably, aftershocks are clustered mainly along the upper, 15° west-dipping segment of the fault model, leaving the lower, 35° (but possibly still 15°) west-dipping part of the rupture almost devoid of events (Figure 1b). We carried out an additional slip inversion with a fault model limited to the upper fault segment 1, which has the same width (30 km) as the aftershock cluster. This model failed at matching the amplitude of the last part of the strong-motion waveforms, showing that strong-motion data require slip to extend more to the west, overreaching the western boundary of the aftershock cluster.

[20] According to the top of the slab boundary located by *Comte and Suárez* [1995], the rupture occurred well inside the plunging plate. Focal mechanisms of intermediate depth earthquakes in various subduction zones worldwide have been interpreted to respond predominantly to down-dip extension (*Isacks and Molnar* [1971] and many later publications), but opposed configurations of the P and T axes have been observed in cases of double seismic zones, notably beneath northern Chile to the south and north of the Tarapaca area [*Comte and Suárez*, 1994; *Comte et al.*, 1999]. However, a precise characterization of the background seismicity at the latitude of the Tarapaca earthquake is lacking, preventing us from analyzing how this event relates to the very local stress regime.

[21] Nonetheless, the Tarapaca event can be interpreted in the more global context of the subduction of northern Chile. The large (Mw 7.8) Tarapaca earthquake is a prominent manifestation of the deformation processes taking place at intermediate depth in response to slab pull and interface locking at shallow depth. It occurred well inside the seismic gap and its T axis is clearly oriented along the dipping direction of the slab. A situation similar to that of the 1950 event, which preceded the 1995 Antofagasta earthquake.

[22] **Acknowledgments.** This work was supported by the Fondecyt 1030800 and ECOS-CONICYT C03U02 programs. We are most grateful to all the staff of the Servicio Sismologico de la Universidad de Chile, and to the personnel of the Departamento de Geofisica for the installation of the temporary network and first processing of the aftershocks, Adriana Perez, Marcel Thielmann, Guillermo Garrido, Jose Escribano, Michel Muñoz, and Patricio Pinares for the final processing of aftershocks as well as for the crustal velocity model. Thanks also to the University of Tarapaca, Bianca Glass, Carlos Leiva and Nebur Alvarez for their analysis of the Tarapaca mainshock with the permanent Arica network RESISTE. Some figures were partly made using GMT package by Paul Wessel and Walter H.F. Smith. We also thank P. Martin Mai and an anonymous reviewer for helpful and accurate comments which allowed us to improve the manuscript.

References

Bouchon, M. (1981), A simple method to calculate Green's functions for elastic layered Media, *Bull. Seismol. Soc. Am.*, *71*(4), 959–971.

Comte, D., and M. Pardo (1991), Reappraisal of great historical earthquakes in the northern Chile and southern Peru seismic gaps, *Nat. Hazards*, *4*, 23–44.

Comte, D., and G. Suárez (1994), An inverted double-seismic zone in Chile: Evidence of phase transformation in the subducted slab, *Science*, *263*, 212–215.

Comte, D., and G. Suárez (1995), Stress distribution and geometry of the subducting Nazca plate in northern Chile using teleseismically recorded earthquakes, *Geophys. J. Int.*, *122*, 419–440.

Comte, D., L. Dorbath, M. Pardo, T. Monfret, H. Haessler, L. Rivera, M. Frogneux, B. Glass, and C. Meneses (1999), A double-layered seismic zone in Arica, northern Chile, *Geophys. Res. Lett.*, *26*(13), 1965–1968.

Delouis, B., D. Giardini, P. Lundgren, and J. Salichon (2002), Joint inversion of InSAR, GPS, teleseismic and strong motion data for the spatial and temporal distribution of earthquake slip: Application to the 1999 Izmit mainshock, *Bull. Seismol. Soc. Am.*, *92*, 278–299.

Kausel, E., and J. Campos (1992), The Ms = 8 Tensional earthquake of December 9, 1950 of northern Chile and its relation to the seismic potential of the region, *Phys. Earth. Planet. Inter.*, *72*, 220–235.

Isacks, B., and P. Molnar (1971), Distribution of stresses in the descending lithosphere from global survey of focal mechanism solutions of mantle earthquakes, *Rev. Geophys.*, *9*, 103–174.

Nabelek, J. (1984), Determination of earthquake fault parameters from inversion of body waves, Ph.D. thesis, 361 pp., Mass. Inst. of Technol., Cambridge, Mass.

Lienert, B. R., E. Berg, and L. N. Frazer (1986), HYPOCENTER: An earthquake location method using centered, scaled, and adaptively damped least squares, *Bull. Seismol. Soc. Am.*, *76*, 771–783.

Okada, T., and A. Hasegawa (2003), The M7.1 May 26, 2003 off-shore Miyagi prefecture earthquake in northeast Japan: Source process and aftershock distribution of an intra-slab event, *Earth Planets Space*, *55*, 731–739.

Peyrat, S., J. Campos, J. B. de Chabalier, A. Perez, S. Bonvalot, M.-P. Bouin, D. Legrand, A. Nercessian, O. Charade, G. Patau, E. Clévédé, E. Kausel, P. Bernard, and J. P. Vilotte (2006), Tarapacá intermediate-depth earthquake (Mw 7.7, 2005, northern Chile): A slab-pull event with horizontal fault plane constrained from seismologic and geodetic observations, *Geophys. Res. Lett.*, *33*, L22308, doi:10.1029/2006GL027710.

Suzuki, S., and M. Kasahara (1996), Unbending and horizontal fracture of the subducting Pacific plate, as evidenced by the 1993 Kushiro-oki and the 1981 and 1987 intermediate-depth earthquakes in Hokkaido, *Phys. Earth Planet. Inter.*, *93*, 91–104.

Yagi, Y., T. Mikumo, J. Pacheco, and G. Reyes (2004), Source rupture process of the Tecoman, Colima, Mexico earthquake of January 22, 2003, determined by joint inversion of teleseismic body wave and near-field data, *Bull. Seismol. Soc. Am.*, *94*(5), 1795–1807.

B. Delouis, Géosciences Azur, CNRS (UMR 6526) and University of Nice, 250 rue A. Einstein, F-06560 Sophia Antipolis, France. (delouis@geoazur.unice.fr)

D. Legrand, Departamento de Geofisica, Universidad de Chile, Blanco Encalada 2002, Santiago, Chile. (denis@dgf.uchile.cl)